MEASUREMENTS OF DIFFERENTIAL DIFFUSION EFFECTS IN TURBULENT MIXING

Cody J. Brownell and Lester K. Su
Department of Mechanical Engineering
The Johns Hopkins University
Baltimore, Maryland 21218, USA
cbrownell@jhu.edu, lsu@jhu.edu

ABSTRACT

Measurements of differential molecular diffusion in a propane-helium jet flowing into air are performed using planar Rayleigh scattering. A comprehensive data set has been obtained for two flow conditions, one at a jet Reynolds number of 1000 and the other at a Reynolds number of 2500. Observations show clear evidence of differential diffusion, particularly in the low Reynolds number case. The standard differential diffusion variable, ξ, is computed and profiles of ξ'_{rms} show similiar features to previous 1-D measurements.

INTRODUCTION

Simulations of turbulent combustion are complicated by the presence of many distinct chemical species, each with different physical properties. A common simplification is to use a single value of molecular diffusivity for all species involved in a system. The assuption is that in a turbulent flow, where inertial effects dominate diffusive effects, the exact nature of molecular diffusion does not change the overall flame structure. For example, it has been shown that the spreading angle of turbulent jets does not depend on the binary diffusivity of the jet and ambient fluids (Chen and Rodi, 1980). The obvious difficulty with this assumption is that chemical reaction requires mixing at the molecular level, where diffusive effects are significant even in turbulent flows. Because the sizes of scalar mixing structures are determined from a balance between strain and diffusion, the range of diffusivities in a reacting flow may make the structure of the mixing field different from one predicted using a uniform diffusivity assumption.

Differential diffusion, defined as the preferential mixing of a scalar with a high diffusivity relative to a scalar with a low diffusivity, has been shown to be an important factor in many reacting flows. Earlier studies involving direct measurement of differential diffusion have been helpful in identifying and measuring its presence in both laminar and turbulent flow fields (Long et al., 1993, Smith et al., 1995). In the present work, we use planar imaging techniques to study differential diffusion in a nonreacting flow. We hope to gain insight into the physical mechanisms of three-species mixing, and to provide information useful for future simulations of turbulent combustion. To accomplish this, we have obtained a comprehensive set of planar measurement data to allow analysis of both statistical and structural properties of differential diffusion.

EXPERIMENTAL METHOD

Planar laser Rayleigh scattering yields direct measurements of differential diffusion in a turbulent axisymmetric jet. The jet fluid is a propane-helium mixture, with the species being chosen for their disparate diffusivities ($D_{C_3H_8} = 0.11$ cm^2/s, $D_{He} = 0.72$ cm^2/s) and for their suitability to this Rayleigh scattering experiment. Rayleigh scattering, a familiar diagnostic method for gas-phase flows, is the elastic scattering of light from molecules or small particles. The Rayleigh scattering signal in a fluid is a function of the intensity of incident light, the local molecular density, and the Rayleigh scattering cross-section. The Rayleigh scattering cross-section, R, of a given species depends on its index of refraction, n, as $R \sim (n-1)^2$; the scattering cross-section of a mixture is the mole fraction weighted average of the cross-sections of constituent species (Eckbreth, 1988). A combination of propane ($n = 1.00109$) and helium ($n = 1.0000349$) can, given the appropriate ratio, create a mixture that has the same Rayleigh scattering cross-section as air ($n = 1.000293$). The resulting mixture has a nominal initial propane mole fraction $\chi^o_{C_3H_8} = 0.071$ and helium mole fraction $\chi^o_{He} = 0.929$.

As this propane-helium jet issues into air, any nonuniformity in the scattering signal is then indicative of local differential diffusion of the propane and helium, i.e. of departure of the propane-helium ratio from the initial value. (This method was originally suggested by Bilger and Dibble (1982) and demonstrated by Long (1993) and Kerstein et al. (1989)). To quantify the measurements, we use the differential diffusion variable ξ, defined in terms of the propane and helium mole fractions as

$$\xi = \frac{\chi_{C_3H_8}}{\chi^o_{C_3H_8}} - \frac{\chi_{He}}{\chi^o_{He}} \tag{1}$$

which can be determined directly from the Rayleigh scattering measurements (Kerstein, 1989). The variable ξ will be greater than zero in regions that have a smaller helium-to-propane ratio than at the jet exit, and will be less than zero in regions that have a larger helium-to-propane ratio. In regions where the ratio is unchanged, and in ambient air, $\xi = 0$.

EXPERIMENTAL ARRANGEMENT

The propane-helium mixture issues from a round pipe with inner diameter $d = 4.6$ mm into a slow ($U_\infty = 0.4$ m/s) filtered air coflow. Filtering with a high-efficiency (HEPA) filter is essential to remove particulates whose presence would contaminate the Rayleigh scattering signal. The light source is a dual cavity Nd:YAG laser (Spectra-Physics PIV-400), capable of approximately 350 mJ per pulse at 532 nm. Both laser cavities are fired during each exposure, making the in-

tensity of incident light approximately 700 mJ per image. The Rayleigh scattering signal is captured by a thermoelectrically-cooled CCD camera (Roper Scientific CoolSNAP HQ), with 1392 × 1040 pixel resolution. In these experiments, the camera is binned to 464 × 346 pixels to increase signal levels and reduce noise. The flow rates of helium and propane are each controlled by a Sierra Instruments C-100 mass flow controller.

Two sets of data are taken, one at a jet-exit Reynolds number of 1000 (Set I), and a second at a Reynolds number of 2500 (Set II). For each set, images are obtained at two different positions in the jet. In the 'near-field' images, the imaging window spans $r = 2.3$ d from the jet centerline in both directions, and extends from $x = 7.0$ d to 10.5 d downstream of the jet exit. In the 'far-field' images, the window covers 3.6 d on either side of the centerline, and extends from 11.3 d to 16.7 d from the nozzle. The pixel spacing is 46 μm for the near-field images, and 72 μm for the far-field images. Each set consists of 6000 total images, split between the two imaging locations.

CALIBRATION AND IMAGE PROCESSING

From preliminary experiments, we found that the results were very sensitive to the exact initial mixture fraction of the jet. We also found that a flow mixed at the theoretical ratio of helium-to-propane (13.02:1) would not produce a mixture with the same Rayleigh scattering cross section as air, due to impurities in the jet gases. An optical calibration was performed to determine the appropriate helium-to-propane ratio for the gas samples used in the experiment. A series of images of a laminar propane-helium jet were obtained in the region immediately above the nozzle. Visible in each image were both the core jet fluid (with composition set by the flow rates of the gases) and ambient air. By varying the initial mixture ratio and comparing the intensity of the Rayleigh scattering signal in the core region to that in the ambient air, we determined that a helium-to-propane ratio of 13.20 to 1 results in a mixture with the same Rayleigh scattering cross-section as air.

To calculate the differential diffusion coefficient ξ from Rayleigh scattering images, the images need to be processed to account for the spatial variation of intensity of incident laser light. Periodically throughout the experiment, Rayleigh scattering images of ambient air are captured that can be averaged and divided, as an effective flat field correction, from the most recent jet images. Images need to be further processed to account for pulse-to-pulse variations from the mean laser profile. The information needed to make this instantaneous correction is contained in the image itself, assuming that the jet width does not exceed the width of the imaging window. By interpolating between profiles of the Rayleigh scattering signal from the ambient air on either side of the jet, we can create an image that represents the instantaneous deviation of the incident laser profile from the previously defined average. Correcting for this instantaneous variation gives an image where the displayed intensity is exactly proportional to the local Rayleigh scattering cross-section of the mixture.

RESULTS

Figures 1 and 2 show sample results for the ξ-field measurements. The jet flows upward in the imaging windows, in the positive x direction. Because the jet fluid is predominantly helium, buoyancy affects the evolution of the mean velocity and jet width, resulting in a local Reynolds number that inreases with downstream distance.

In Set I, shown in Fig. 1, the jet is initially laminar and undergoes the transition to turbulence immediately below the bottom of image (a). Previous results have found clear divisions within the cross-section of a differentially diffusing laminar jet. Specifically, in the laminar core there is a region of jet fluid that has not seen any substantial changes in its relative propane-helium concentration. The outermost radial layer is a wide ring of helium-rich fluid, which has diffused radially farther than the propane. Immediately outside the core there is a region of propane-rich fluid, created primarily by an absence of the fast-diffusing helium. In the current images from Set I, large coherent regions of both helium- and propane-rich fluid are visible in the turbulent jet. It is likely that many of these regions were created from differential diffusion during the laminar phase, and have been clipped off and advected downstream into the turbulent region.

Image (b) in Fig. 1 is another instantaneous image from Set I, but looking farther downstream than image (a). Typical of images from this location, the regions of helium- and propane-rich fluid are still obvious, but have diminished somewhat in their overall size and intensity. Unlike the laminar portion of the jet, there are no clearly identifiable regions that, averaged over time, are consistently rich in either helium or propane.

The images in Fig. 2 are from Set II, at the near- and far-field locations, respectively. This set is inherently different from the jet in Set I due to an absence of any significant laminar characteristics near the jet exit. Still, there is significant evidence of differential diffusion throughout both images. Regions of non-zero ξ appear at various points in the flow, although the structures are on average smaller than those from Set I. In this flow, all deviations from the original helium-propane ratio must have formed in flow regions characterized by at least moderate turbulence.

STATISTICAL ANALYSIS

For each data set, we have computed probability density functions for ξ at different radial positions throughout the jet. In the near-field images, statistics were obtained from points in regions A, B, and C, shown in Fig. 3. Region A is along the jet centerline, and regions B and C are centered at $r/d = 1$ and $r/d = 2$, respectively. In the far-field images four different regions were used, as shown in Fig. 3, starting with region D on the centerline and then moving outward one nozzle diameter for successively regions E,F, and G.

In the near-field statistics for Set I (Fig. 4), we can see a dramatic difference between the PDF from region C, an area that typically sees no jet fluid, and those from regions A and B that are within the jet boundaries. While the variations seen in region C are attributed to noise, the difference between it and the other two regions is the result of fluctuations in ξ caused by differential diffusion between the helium and the propane. It is also noteworthy that the peak for region A lies slightly above zero, while the peak for region B is below zero. This shows that the helium has spread farther from the jet centerline than the propane, an effect that is likely exaggerated by the pre-existing laminar diffusion. In the far-field these same features are observed, with the primary difference being the convergence of the statistics as all species are given more time to mix.

The near-field statistics for Set II, shown in Fig. 5(a), are

qualitatively different from those in the lower Reynolds number case. The three PDFs are more consistent, due to the increased turbulent mixing in this flow. We also observe that the PDF that peaks at the highest value of ξ is in region C, on the outside of the jet. This implies a greater prevalence of the slower-diffusing propane on the outside of the jet, a counter-intuitive observation but one that was also seen in experiments by Kerstein et al. (1989). In the far-field, Fig. 5(b), there is further convergence of the different PDFs, although the greater prevalence of propane on the outside of the jet appears to persist.

RMS FLUCTUATIONS

The RMS fluctuations of ξ,

$$\xi'_{rms} = \left(\overline{(\xi_n - \xi_{mean})^2}\right)^{1/2} \quad (2)$$

have been computed for Set I and are shown shown in Fig. 6. The background noise has been subtracted from these images to show only variations in ξ. (Results from Set II have been omitted due to space restrictions.) In the near field, we can again see residual features from the prior laminar jet, this time in a bimodal form of the ξ'_{rms} profile. The two peaks are present at the bottom of the image and extend to approximately 8.5 diameters downstream. It is over this region that we expect to see the largest fluctuations in ξ due to coherent regions of helium- or propane-rich fluid being advected through. As the flow field becomes more turbulent, these peaks are quickly smoothed over, and by $x = 9$ d, the ξ'_{rms} profile is very uniform across the entire jet width (Fig. 7). From the far-field images, we can see that as the flow evolves further this uniform profile gives way to a second bimodal structure. Here, peak values of ξ'_{rms} are located on the edges of the jet, while the jet centerline sees consistent but smaller fluctuations. Measurements of ξ'_{rms} from Set II (not shown) also confirm this structure. These results showing a bimodal structure in ξ'_{rms} beyond the region affected by laminar flow are confirmed by previous results of Kerstein et al. (1989) and Bilger and Dibble (1982).

Observing the evolution of ξ'_{rms} along the centerline, and in particular the decrease of ξ'_{rms} with increasing x, is helpful in determining the rate at which regions of non-zero ξ are dissipated. Although comparisons with the velocity field and local Reynolds number cannot be made at this time, it is clear that the decay is measurable and further insight will be provided by velocity field measurements in this flow.

CONCLUSIONS

Results from differential diffusion imaging of a propane-helium jet issuing into air confirm that differential diffusion is significant in turbulent shear flows. Once present, differential diffusion structures are advected and slowly dissipated in the turbulent velocity field. The degree to which differential diffusion occurs is affected by the Reynolds number of the flow, but a quantitative description of this relationship is not yet available. The RMS fluctuations of the differential diffusion variable ξ are computed over the 2-D measurement regions, and confirm previous 1-D experimental and computational results. Ongong work involves quantifying the velocity field of the present flow, analyzing the spatial spectra of the ξ field, and on obtaining a more thorough description of the formation and dissipation of differential diffusion structures within the flow.

REFERENCES

Bilger, R.W., 1981, "Molecular transport effects in turbulent diffusion flames at moderate Reynolds number", Paper 81-0104, AIAA 19th Aerospace Sciences Meeting, St. Louis, MO.

Bilger, R.W. and Dibble, R.W., 1982, "Differential molecular diffusion effects in turbulent mixing", *Combustion Science and Technology*, Vol. 28, pp. 161-172.

Brownell, C.J. and Su, L.K., 2004, "Planar measurement of differential diffusion in turbulent jets", Paper 2004-2335, 34th AIAA Fluid Dynamics Conference and Exhibit, Portland, OR.

Chen, C.J., and Rodi, W., 2000, **Vertical Turbulent Buoyant Jets: A Review of Experimental Data**, Pergamon, Oxford, UK.

Eckbreth, A., 1988, **Laser Diagnostics for Combustion Temperature and Species**, Abacus Press, Kent, UK.

Hilbert, R., and Thevenin, D., 2004, "Influence of differential diffusion on maximum flame temperature in turbulent nonpremixed hydrogen/air flames", *Combustion and Flame*, 138, pp. 175-187.

Kerstein, A.R., Dibble, R.W., Long, M.B., Yip, B., and Lyons, K., 1989, "Measurement and computation of differential molecular diffusion in a turbulent jet", Seventh Symposium on Turbulent Shear Flows, Stanford, CA.

Long, M.B., 1993, "Multidimensional imaging in combusting flows by Lorenz-Mie, Rayleigh and Raman scattering", In **Instrumentation for Flows with Combustion**, Academic Press.

Long, M.B., Starner, S.H., and Bilger, R.W., 1993, "Differential diffusion in jets using joint PLIF and Lorenz-Mie imaging", *Combustion Science and Technology*, Vol 92, pp. 209-224

Pope, S.B., 2000, **Turbulent Flows**, Cambridge University Press, UK.

Smith, L.L., Dibble, R.W., Talbot, L., Barlow, R.S., and Carter, C.D., 1995, "Laser Raman scattering measurements of differential molecular diffusion in nonreacting turbulent jets of H_2/CO_2 mixing with air", *Physics of Fluids*, Vol 7, pp. 1455-1466.

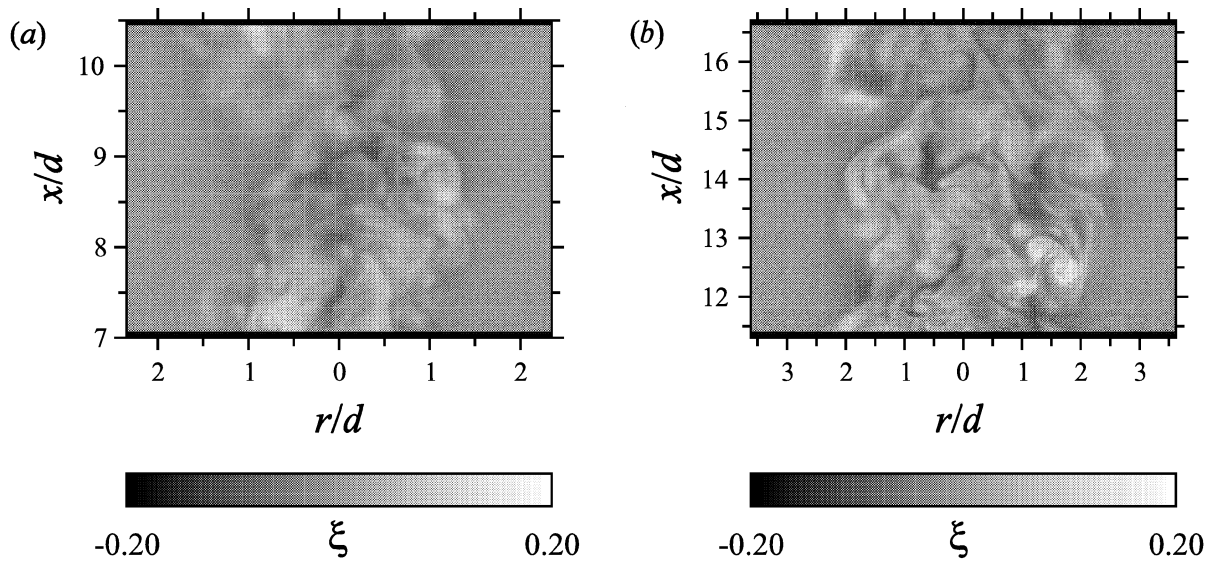

Figure 1: Two sample images from a low Reynolds number (Re = 1000) turbulent jet (Set I) show significant differential diffusion structures throughout all parts of the flow. Image (a) spans from 7.0 to 10.5 jet diameters downstream, while image (b) shows $x = 11.3\ d$ to $16.7\ d$

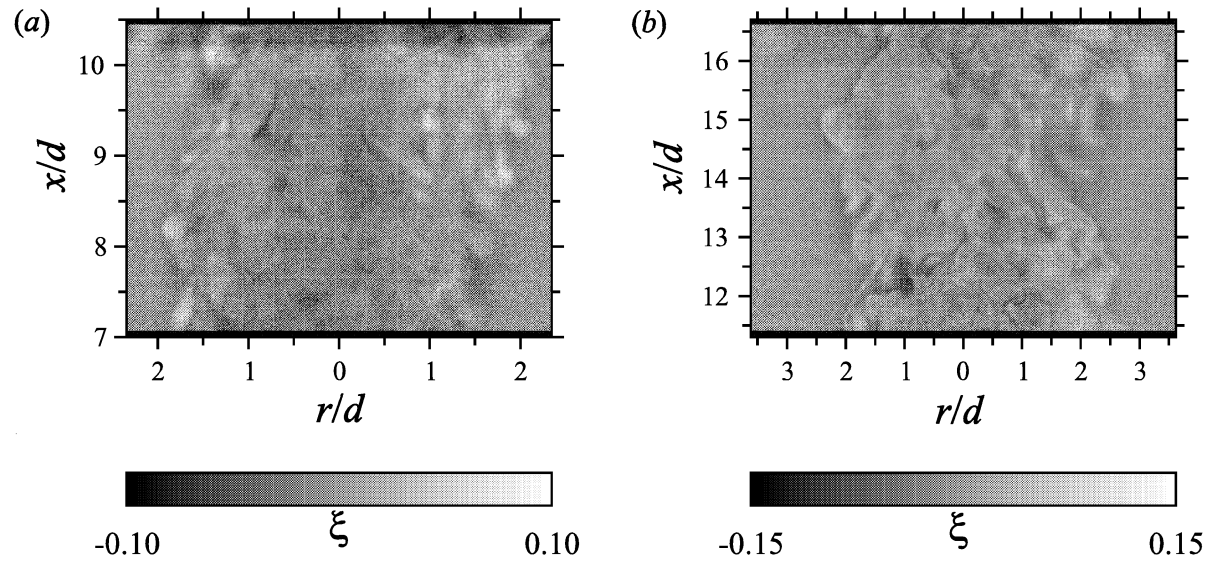

Figure 2: Sample images from Set II, a moderate Reynolds number jet (Re = 2500), show many of the same features as seen in Fig. 1 for both the near-field (a) and far-field(b), although the average magnitude of ξ is significantly less due to the increased turbulent mixing in this flow.

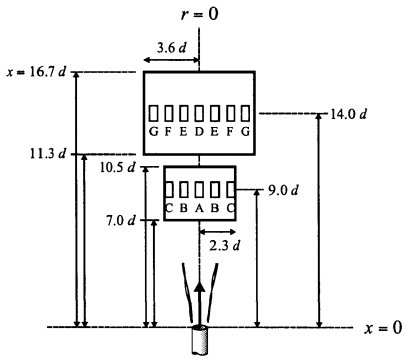

Figure 3: The location of the imaging areas relative to the nozzle, and the relative sizes of the imaging windows. Probability density functions of the ξ-field were computed in the regions designated A to G.

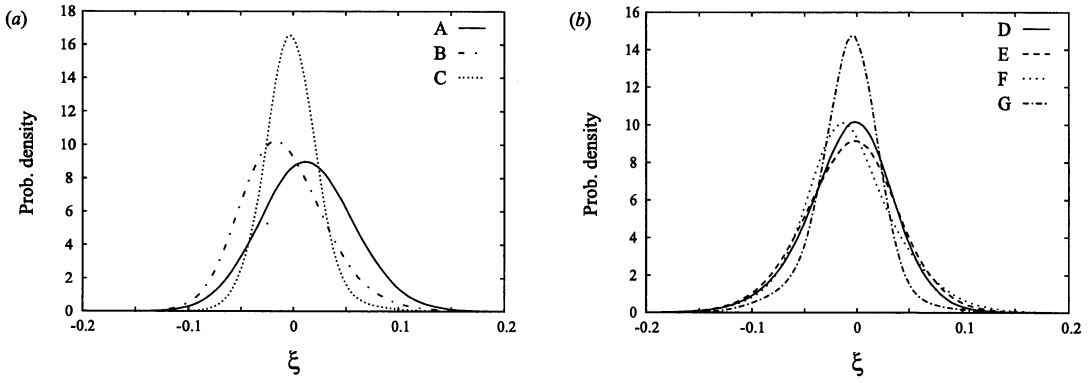

Figure 4: Cross-stream probability density functions from Set I show a clear difference between the statistics obtained from the in-jet regions (A,B,D,E,and F) and those obtained outside the jet boundaries (C and G). Within the jet, propane-rich fluid is more common along the centerline and helium-rich fluid is more common on the perimeter.

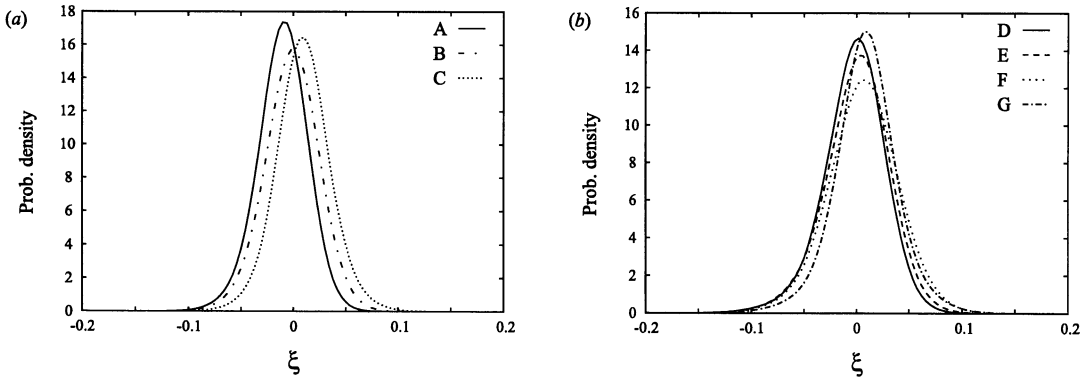

Figure 5: Cross-stream probability density functions from Set II are somewhat different from their low Reynolds number counterparts. As this jet was wider than the jet in Set I, regions C and G cannot be assumed to be outside of the jet flow. Contrary to the results from Set I, these statistics show a preference for propane-rich fluid on the perimeter and helium-rich fluid near the center of the jet.

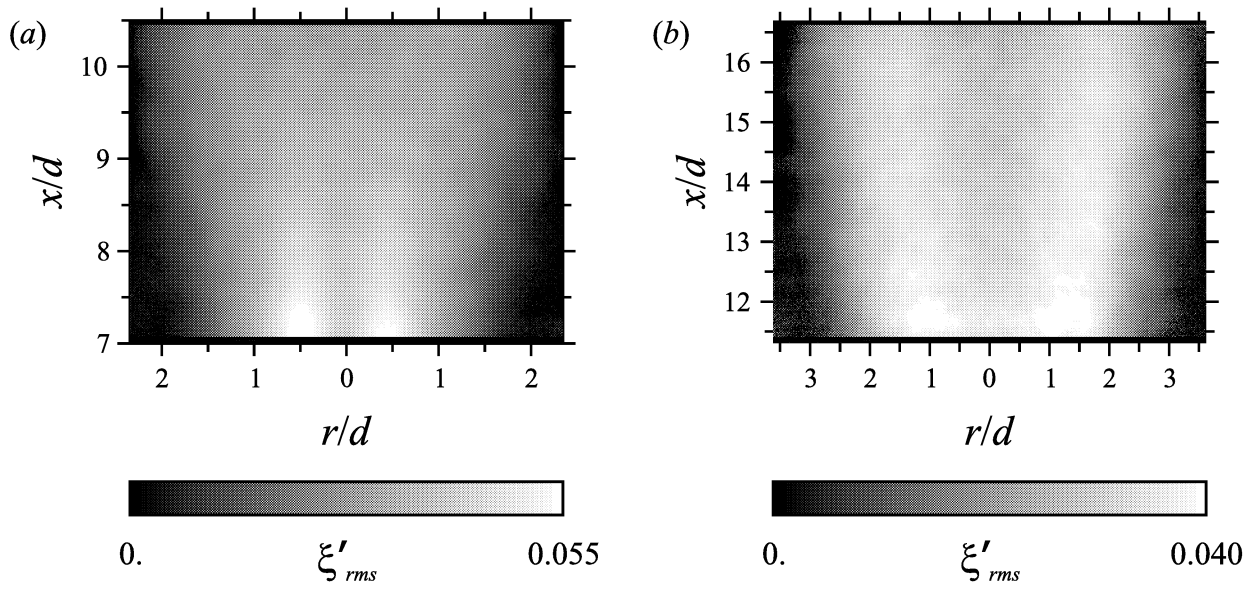

Figure 6: Calculations of ξ'_{rms} for Set I show strikingly different features at different positions within the flow. Just downstream from the laminar flow region, there are two sharp peaks in the ξ'_{rms} profile that are quickly leveled by the turbulent velocity field. Farther downstream, however, a second bimodal structure forms, suggesting that the greatest fluctuations in ξ occur near the outside of the jet and not on the centerline.

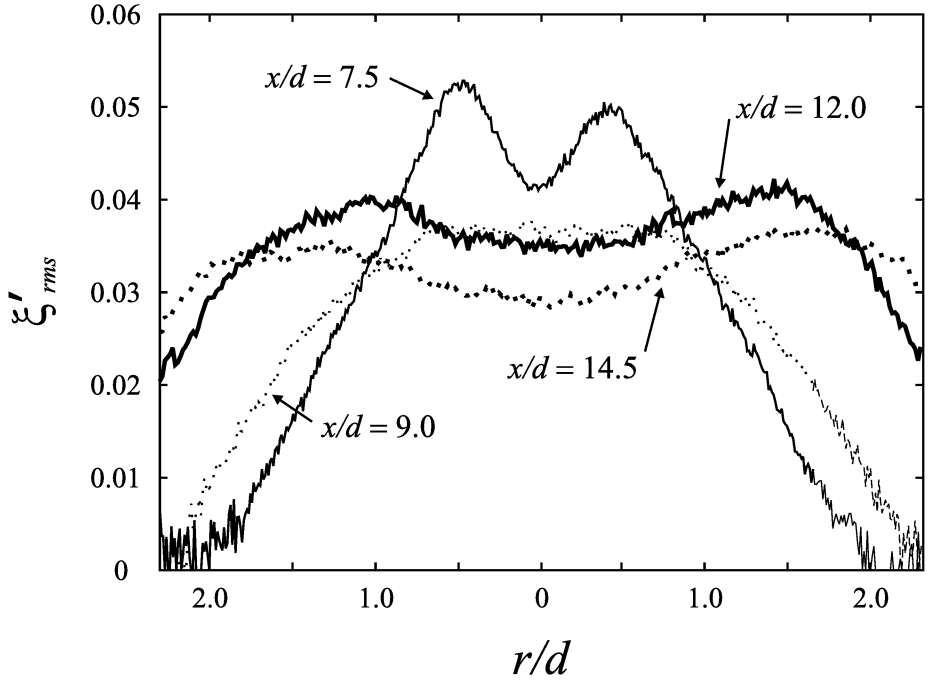

Figure 7: Profiles of ξ'_{rms} from Set I at various downstream positions give a clearer picture of the effect of turbulence on differential diffusion. As shown in Fig. 6, bimodal structures exist in both the near-field and far-field regions. The steady decay in ξ'_{rms} along the centerline is also apparent from these profiles.